

Decadal-scale rainfall variability in Ethiopia recorded in an annually laminated, Holocene-age, stalagmite

The Holocene
20(6) 827–836
© The Author(s) 2010
Reprints and permission:
sagepub.co.uk/journalsPermissions.nav
DOI: 10.1177/0959683610365934
http://hol.sagepub.com
SAGE

Andy Baker,^{1,2} Asfawossen Asrat,³ Ian J. Fairchild,² Melanie J. Leng,^{4,5}
Louise Thomas,⁶ Martin Widmann,² Catherine N. Jex,² Buwen Dong,⁷
Peter van Calsteren⁶ and Charlotte Bryant⁸

Abstract

An annually laminated, uranium-series dated, Holocene stalagmite from southeast Ethiopia has been analysed for growth rate and $\delta^{13}\text{C}$ and $\delta^{18}\text{O}$ variations at annual to biennial resolution, in order to provide the first long duration proxy record of decadal-scale rainfall variability in this climatically sensitive region. Our study site (10°N) is climatically influenced by both summer (June–August) and spring (March–May) rainfall caused by the annual movement of the Inter-Tropical Convergence Zone (ITCZ) and modulated by large-scale anomalies in the atmospheric circulation and in ocean temperatures. Here we show that stalagmite growth, episodic throughout the last 7800 years, demonstrates decadal-scale (8–25 yr) variability in both growth rate and $\delta^{18}\text{O}$. A hydrological model was employed and indicates that this decadal variability is due to variations in the relative amounts of rainfall in the two rain seasons. Our record, unique in its combination of length (a total of ~1000 years), annual chronology and high resolution $\delta^{18}\text{O}$, shows for the first time that such decadal-scale variability in rainfall in this region has occurred through the Holocene, which implies persistent decadal-scale variability for the large-scale atmospheric and oceanic driving factors.

Keywords

Ethiopia, Holocene, rainfall, speleothem

Introduction

The African climate system, including its monsoons, is a key element of the global atmospheric circulation. Much remains to be understood about the links between the African climate and the variability of the surrounding oceans and atmosphere, as well as the hemispheric- and global-scale climate. Our study site in the Ethiopian highlands is a classic example of an African rain-sensitive region, where seasonal forecasts and climate change predictions are hampered by inadequate understanding of historical patterns, their wider associations and causes. Spring rainfall failures can lead to drought, while excessive summer rains such as in 2007, cause flooding over most of Northern Hemisphere tropical Africa, including Ethiopia. The reasons for the interannual variability in spring and summer rainfall are only partly understood, and vary strongly between different regions in Ethiopia (Camberlin and Philippon, 2002). Rainfall and temperature records are relatively short and of poor quality (Conway *et al.*, 2004). The few long records demonstrate that after El Niño years, the spring rains tend to be strong and the main summer rains are reduced (Glantz, 1996). This agrees with a strong multiyear spectral peak in rainfall records for the region that is also found in Atlantic and Indian Ocean sea surface temperatures (SSTs) (Nicholson, 2000). A weak or late start of the spring rainfall has been linked to a cool tropical North Atlantic (Rowell *et al.*, 1994). Spring rain is also influenced by atmospheric circulation anomalies that extend from Western Europe to the Arabian Peninsula, and which are associated with shifts in the subtropical jet stream, and low-level moisture

influx and large-scale convection over Ethiopia (Camberlin and Philippon, 2002). To what extent these atmospheric anomalies are related to SST anomalies have not yet been investigated. As a consequence of the poor ENSO predictability in the Northern Hemisphere spring and of the presence of these additional influences on Ethiopian rainfall, attempts to predict interannual rainfall variability in summer (Block and Rajagopalan, 2007; Korecha and Barnston, 2007) and spring (Diro *et al.*, 2008) have shown only limited skill. Under future climate change, models predict an enhanced seasonal precipitation range in the tropics (Chou *et al.*, 2007).

¹The University of New South Wales, Australia

²University of Birmingham, UK

³Addis Ababa University, Ethiopia

⁴NERC Isotope Geosciences Laboratory, British Geological Survey, UK

⁵University of Nottingham, UK

⁶The Open University, UK

⁷University of Reading, UK

⁸NERC Radiocarbon Facility (Environment), UK

Received 13 July 2009; revised manuscript accepted 4 January 2010

Corresponding author:

Andy Baker, The University of New South Wales, 110 King St, Manly Vale, NSW2093, Australia

Email: a.baker@unsw.edu.au

As the instrumental series are too short to investigate low-frequency rainfall variability and its links to large-scale climate variability, long, high temporal resolution climate estimates from proxies are therefore required. To this aim, we have analysed an annually laminated stalagmite record from SE Ethiopia. Previous annually laminated stalagmites from the region have been analysed for the Modern period (Baker *et al.*, 2007) and the mid-Holocene (Asrat *et al.*, 2007), and cave sites in the region have undergone extensive exploration (Baker *et al.*, 2005; Gunn *et al.*, 2009) and monitoring (Asrat *et al.*, 2008) over the last five years. Here, we present annual growth rate variations and annual–biennial resolution variations in $\delta^{18}\text{O}$ for a stalagmite that has grown discontinuously through the Holocene, with the timing of growth constrained by uranium-series and radiocarbon analyses.

Materials and methods

Stalagmite Bero-1 was collected from Bero Cave, SE Ethiopia (37°E, 09°N, altitude 1363 m a.s.l.) in 2005. Bero-1 was being actively dripped upon (30 s/drip) when collected in October 2005 from Bero Cave. Drip rate was subsequently recorded as 8 min/drip in June 2006. The cave is near the base of a 61 m high cliff of massive crystalline limestone; full regional and local cave descriptions and geochemistry can be found in Asrat *et al.* (2008).

When sliced, Bero-1 revealed sections of annual laminae packaged into continuous units separated by hiatuses which represent growth phases of ~80–300 years (Figure 1). Lamina counting was conducted on a scanned high-resolution image of the polished stalagmite using image processing software (Image Pro Plus 5.0) using the protocols previously outlined (Tan *et al.*, 2006). The image was enhanced, by stretching the observed range of pixel intensities to the maximum possible (full 0–255 range), and lamina thicknesses calculated by measuring the average distance between visible laminae using a ~50 pixel wide transect. Triplicated lamina profiles were counted. Growth rate was derived from visible lamina thicknesses.

Overall, Bero-1 comprised six growth phases; the oldest five were dated using uranium-series analyses and the most recent growth phase was analysed by ^{14}C . Uranium-series analyses were carried out at the Open University (UK): speleothem samples (typically 0.5 g) were totally dissolved and spiked with a mixed $^{229}\text{Th}/^{236}\text{U}$ spike. Uranium and thorium fractions were separated on 2 ml anion exchange columns using standard techniques (Edwards *et al.*, 1987). Uranium fractions were loaded onto graphite coated Re filaments and analyses carried out using a Finnigan MAT262 mass spectrometer equipped with a retarding potential quadrupole and secondary electron multiplier. A dynamic peak-switching routine was employed measuring $^{234}\text{U}/^{236}\text{U}$ and $^{235}\text{U}/^{236}\text{U}$ (a proxy for ^{238}U , assuming a $^{238}\text{U}/^{235}\text{U}$ natural ratio of 137.88), whilst the Thorium samples were diluted to approximately 10 ppb and run on the NU plasma Multi-Collector Inductively Coupled Plasma. A dynamic peak-switching routine was employed measuring $^{230}\text{Th}/^{229}\text{Th}$ and $^{232}\text{Th}/^{229}\text{Th}$. ^{232}Th abundance was measured in order to monitor detrital Th input and consequently correct for its presence if required. A standard-sample bracketing technique was used for the Nu plasma in order to monitor and if necessary correct for drift. Two internal solution standards and one rock standard were used to assess external reproducibility. Two total procedure blanks (run in parallel with these samples) for ^{238}U and ^{232}Th yielded 8 pg and 12 pg, respectively. These blanks are negligible for the samples measured and, as for the apparent blank contribution for the ^{232}Th concentrations

of the samples, this is less than 1% for most samples but ~2% for the samples that require the smallest ^{232}Th correction.

The ^{14}C activity of modern speleothems is used to confirm the active deposition, and this technique was utilized on the modern growth phase of the sample. Stalagmites record the atmospheric ^{14}C bomb input superimposed on the ^{14}C signal from ‘dead carbon’ that has derived from limestone dissolution. Stalagmite ‘dead carbon proportion’ is typically 15±10% (Genty *et al.*, 2001), and the superimposed ‘bomb carbon’ signal is both damped and has a time delay between 1964 (date of the atmospheric ^{14}C peak) and the maximum of ^{14}C activity observed in the stalagmite, due primarily to soil carbon cycling. Speleothem samples were drilled at locations shown on Figure 1 and stored under argon until hydrolysis to CO_2 using 85% H_3PO_4 at 25°C. Carbon dioxide was cryogenically separated. Aliquots of CO_2 were converted to an iron/graphite mix by iron/zinc reduction (Slota *et al.*, 1987). A subsample of CO_2 was used to measure $\delta^{13}\text{C}$ using a dual-inlet mass spectrometer with a multiple ion beam collection facility (VG OPTIMA) in order to normalise ^{14}C data to -25‰ $\delta^{13}\text{C}_{\text{VPDB}}$. Graphite prepared at the NERC Radiocarbon Laboratory was analysed by Accelerator Mass Spectrometry at the Scottish Universities Environmental Research Centre AMS (5MV NEC).

Finally, samples were taken for carbon and oxygen isotope analysis. For the majority of the sample, these were drilled at regular intervals along the central growth axis of the speleothem (see Figure 1). To avoid aliasing effects, we drilled time-integrated samples of 1–2 years (~1 mm) duration. However, in order to best understand the modern behaviour of growth rate and $\delta^{18}\text{O}$ in the stalagmite, the top most sample was milled at 100 μm resolution using a New Wave Research micromill, yielding samples of approximately 2–3 months duration for the last ~30 years. In addition, samples were drilled laterally along growth laminae, in order to investigate the lateral changes in isotope composition (the ‘Hendy test’, labelled H1–H11 on Figure 1). Analyses were conducted at the NERC Isotope Geosciences Laboratory at Keyworth. The calcite samples were reacted with phosphoric acid and cryogenically purified before mass spectrometry using an Isoprime plus multiprep dual inlet mass spectrometer. By comparison with a laboratory marble standard, the sample $^{18}\text{O}/^{16}\text{O}$ and $^{13}\text{C}/^{12}\text{C}$ ratios are reported as $\delta^{18}\text{O}$ and $\delta^{13}\text{C}$ values in per mil (‰) versus VPDB. Analytical precisions are 0.07‰ for $\delta^{18}\text{O}$ and 0.04‰ for $\delta^{13}\text{C}$ on the standard marble (KCM).

Results

Laminae and geochemistry

The laminated but discontinuous growth of Bero-1 is typical of stalagmites in the region, where the strong seasonality of rainfall encourages annual lamina formation (Asrat *et al.*, 2007; Baker *et al.*, 2007), and the tectonic instability of the region (close to the E African rift) is inferred to create variations in drip water flux and therefore growth phases of relatively short duration. In thin-section, infiltration laminae are observed as elsewhere in the region (Baker *et al.*, 2007); these submillimeter-scale laminae visible in both hand and thin section (see inset, Figure 1) are defined by zones with multiple thin (micron-scale) laminae represented by impurities (opaque in transmitted light) reflecting multiple pulses of infiltration in response to rain events. Where most strongly developed they drape crystallite surfaces that occasionally show some dissolution features. We thus interpret the laminae as representing seasonally high flows.

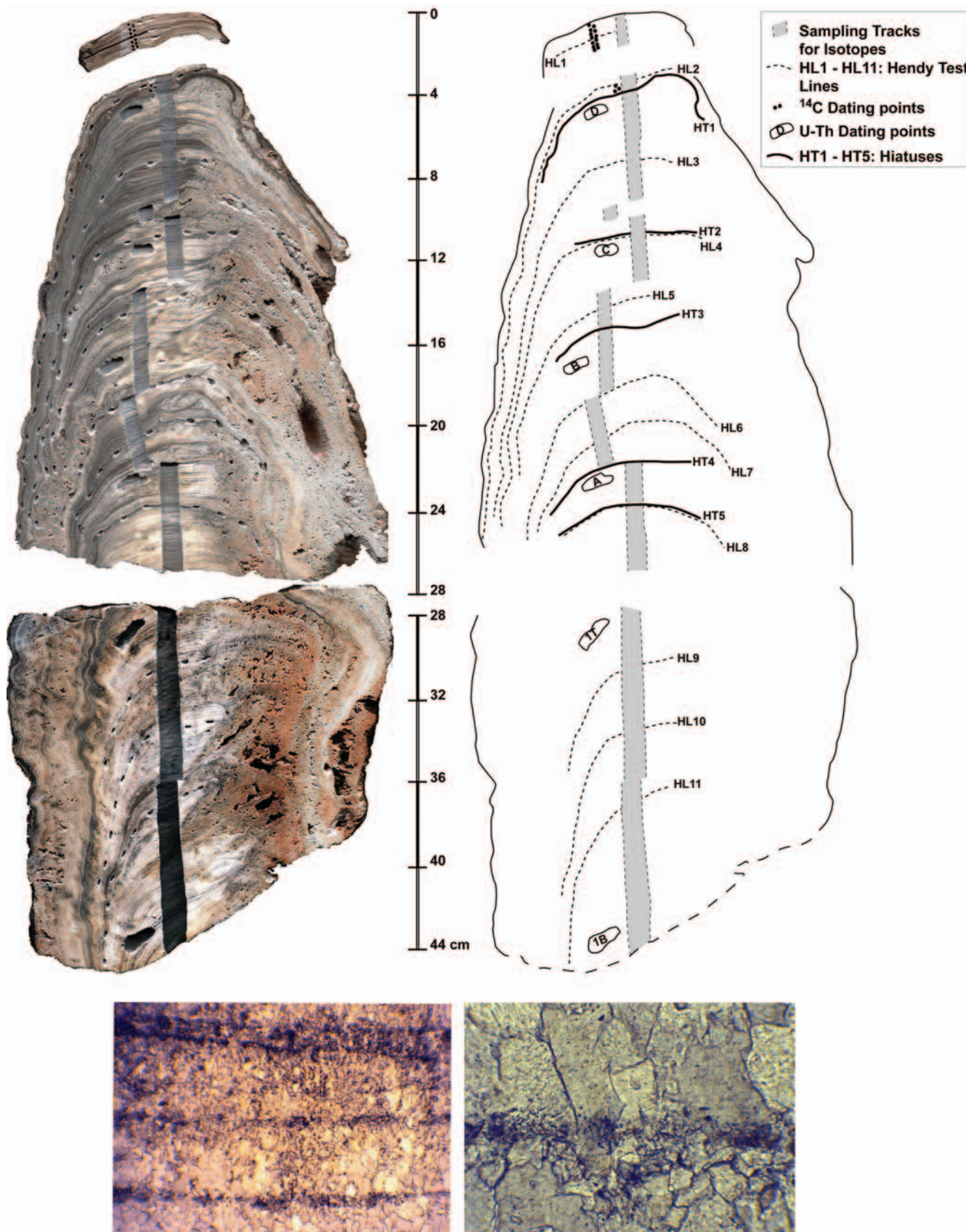


Figure 1. Bero-I hand-section in both photograph (left) and sketch (right), showing location of growth hiatuses, and sampling for U-Th, ^{14}C and $\delta^{13}\text{C}$ and $\delta^{18}\text{O}$ analyses. Bottom: thin-section examples of annual laminae (bottom left, height of image 3.5 mm) and high resolution image of one lamina showing seasonal change in fabric coinciding with deposition of organic matter (bottom right, height of image 0.85 mm)

Radiometric results (see Table 1), combined with annual lamina counting, show that the stalagmite grew over the periods ~7.8–7.3, ~5.9, ~5.4–5.3, ~4.8, ~4.3–4.2 ka and the last ~30

years. For the latter period, substantial soil and groundwater carbon storage and mixing is indicated by the lack of a strong ‘bomb’ ^{14}C peak (Genty et al., 2001). Table 1 demonstrates that for

Table 1. U-Th (top) and ¹⁴C (bottom) analytical data. Ages are given in years before analysis (AD 2007)

	Bero D	Bero C	Bero B	Bero A	Bero 1T	Bero 1B
²³⁸ U ppm	0.0926	0.0555	0.0573	0.0611	0.1406	0.0602
uncertainty	0.0002	0.0001	0.0001	0.0001	0.0002	0.0001
(²³⁴ U/ ²³⁸ U)	1.1894	1.2220	1.2003	1.1787	1.1923	1.2219
uncertainty	0.0071	0.0082	0.0055	0.0045	0.0063	0.0109
²³⁴ U ppm	5.9403E-06	3.6622E-06	3.7108E-06	3.8866E-06	9.0431E-06	3.9676E-06
uncertainty	3.4822E-08	2.4301E-08	1.6680E-08	1.4685E-08	0.00000005	0.00000003
²³⁰ Th ppb	8.6953E-05	5.3332E-05	5.8775E-05	7.0686E-05	2.0838E-04	9.7222E-05
uncertainty	1.2520E-06	7.2744E-07	9.9370E-07	9.8655E-07	0.000002	0.000001
²³² Th ppb	3.05	1.08	1.07	1.81	5.398383	2.904741
uncertainty	0.55	0.20	0.19	0.33	0.975844	0.525078
(²³⁰ Th/ ²³² Th)	10.9566	23.5192	25.1638	16.2270	8.7905	8.2315
uncertainty	0.5158	1.0894	1.2477	0.7567	0.3834	0.3744
(²³⁰ Th/ ²³⁴ U)	0.04826	0.04801	0.05222	0.05996	0.07596	0.08078
uncertainty	0.00070	0.00066	0.00088	0.00084	0.00083	0.00104
(²³⁴ U/ ²³⁸ U)	1.18943	1.22202	1.20033	1.17866	1.19225	1.22193
uncertainty	0.00710	0.00823	0.00552	0.00455	0.00626	0.01094
Uncorrected age	5394	5365	5848	6742	8610	9175
2 σ uncertainty	159	150	203	194	195	244
2 σ uncertainty	-159	-150	-203	-194	-195	-244
%err 2se	2.95	2.79	3.47	2.87	2.27	2.66
Corrected age	4397	4794	5289	5838	7451	7754
2 σ uncertainty	184	189	259	237	239	293
2 σ uncertainty	-184	-190	-260	-237	-239	-293
%err 2se	4.17	3.95	4.91	4.07	3.21	3.78

(ages corrected using a detrital ²³²Th/²³⁸U of 3.12)

Publication code	Sample ID	¹⁴ C Enrichment % modern ± 1σ	Absolute % modern ^a	Conventional radiocarbon age ± 1σ	Lamina age (yr BP ± 1σ)	δ ¹³ C(VPDB) ± 0.1‰
SUERC-12965	Bero-1 A	86.33 ± 0.38	85.77 ± 0.38	1181 ± 35	AD 2005	-5.0 ^b
SUERC-12966	Bero-1 B	84.52 ± 0.37	83.97 ± 0.37	1351 ± 35	AD 2000	-5.0
SUERC-12967	Bero-1 C	85.53 ± 0.37	84.98 ± 0.37	1255 ± 35	AD 1990	-5.7
SUERC-12968	Bero-1 D	84.29 ± 0.37	83.74 ± 0.37	1373 ± 35	AD 1980	-4.3
SUERC-12969	Bero-1 E	82.89 ± 0.36	82.35 ± 0.36	1507 ± 35	AD 1970	-4.3
SUERC-12970	Bero-1 F	50.63 ± 0.23	50.30 ± 0.23	5468 ± 35	~2400 BC	-0.1

^aAbsolute % modern involves a mathematical adjustment to account for ongoing radioactive decay of the international reference standard (oxalic acid) since AD 1950.

^bValue estimated as insufficient material for independent δ¹³C analysis.

Bero-1F, sampled at the same growth phase as U-Th dated to ~4.3–4.2ka, that for this time period at least the ‘dead carbon proportion’ was ~20–25%. Bero-1A to 1E, with absolute %modern values of 82–86%, are therefore indicative of post ‘bomb carbon’ deposition.

Palaeoclimate proxies were obtained from the determination of annual growth rate from the mean of triplicate lamina thickness measurements, and stable isotope (δ¹³C, δ¹⁸O) determinations at annual to biennial resolution. Time series of δ¹⁸O and growth rate are shown in Figure 2; analysis of δ¹⁸O versus δ¹³C variability is presented in Figure 3. The latter show covariation between the isotopes both along a growth lamina (the ‘Hendy test’) and through time, typically interpreted as being indicative of disequilibrium conditions, with the δ¹³C/δ¹⁸O gradient of 0.5–2.4 for ‘Hendy tests’ agreeing well with experimental data for rapid degassing (1.4±0.6) (Wiedner *et al.*, 2008). Growth rate and δ¹⁸O time series (Figure 2) show the following characteristics:

(1) Subannually resolved, milled samples, over the last ~30 years demonstrate variable intra-annual δ¹⁸O variability, ranging from 0.1 to > 1‰, which is smoothed by our integrated drilling for the rest of the sample.

- (2) 1–2 yr integrated δ¹⁸O samples exhibit decadal-scale variability of ~1–3‰ throughout the Holocene. This is superimposed onto a long-term variation in δ¹⁸O, with lighter δ¹⁸O earlier in the record.
- (3) Growth rate also exhibits decadal-scale variability but with noticeable inter-year variability and clear evidence of non-linear, short duration, increases in growth rate.

Forward modelling of stalagmite oxygen isotopes

Stalagmite response to surface climate forcing is controlled by the hydrology of the drip-water, which in karst aquifers can comprise multiple flow routes and non-linear behaviour (Fairchild *et al.*, 2006; Smart and Friederich, 1987). Isotope and growth rate responses for modern growth may be explored using linear regression against instrumental climate series (Baker and Bradley, 2010; Baker *et al.*, 2007). However, the short duration of modern growth (<40 years), coupled with the possibility of a smoothed and lagged groundwater component (reducing the already limited degrees of freedom) and the possible non-linear behaviour of karst ground water, preclude this approach. Instead, oxygen isotope responses are forward modelled. The forward model permits the mixing of

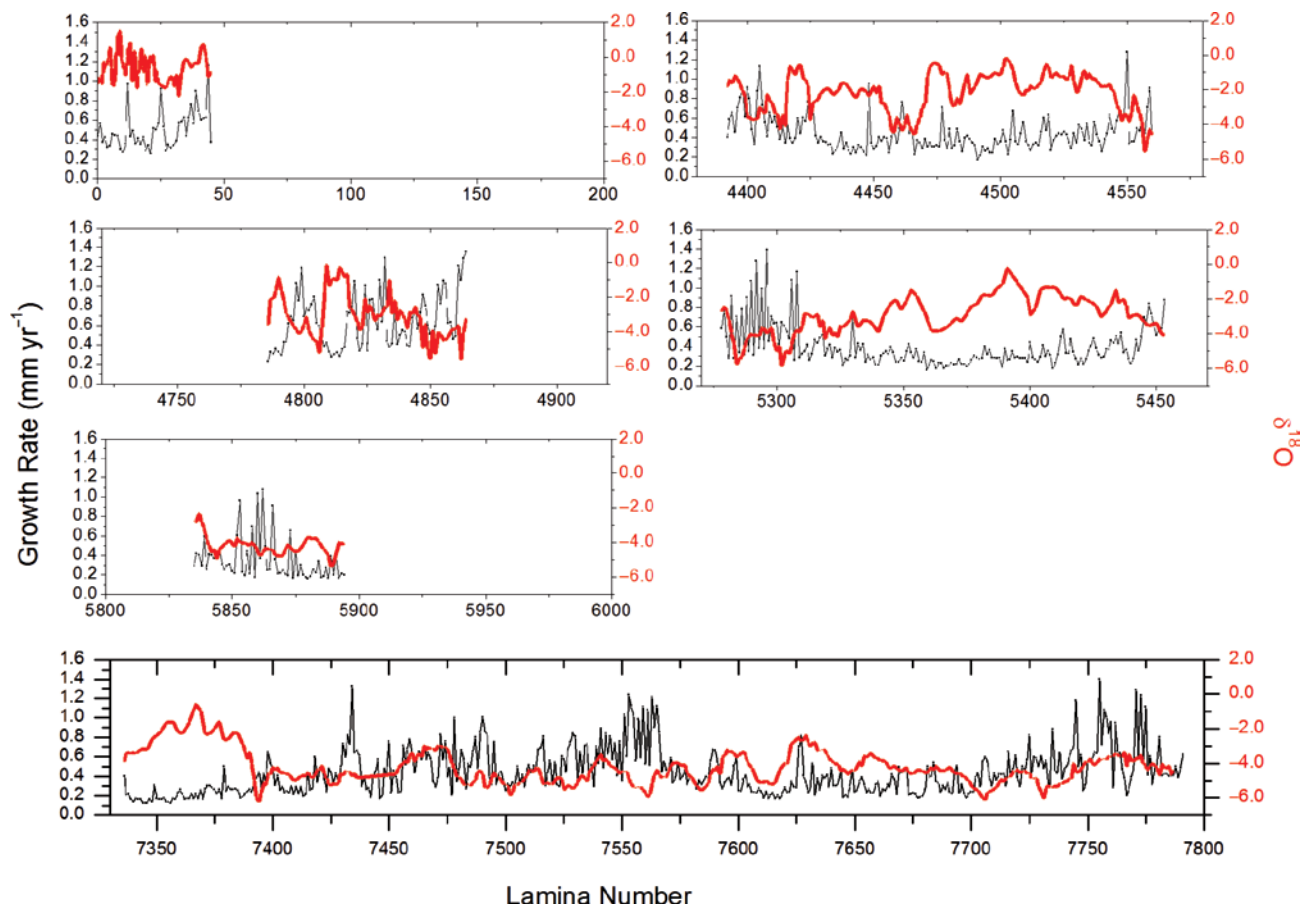


Figure 2. Growth rate (left axis, thin line) and $\delta^{18}\text{O}$ (right axis, thick line) time series for Bero-I for all six growth periods. The chronology is given as lamina number, where year 0 is the year of sampling (AD 2005) and the lamina number approximates to the time of deposition determined by U-Th analyses (Table 1). Note that the uncertainty associated with the U-Th ages means that the lamina numbers cannot be interpreted as precise calendar ages

the isotope signatures of monthly rainwater using Addis Ababa monthly isotope samples archived in the IAEA WISER data base. The model incorporates two hydrological thresholds for water infiltration into the seepage reservoir and into fracture-fed flow, respectively, which reflects our observed infiltration laminae (see Figure 5a). Water entering the seepage reservoir has a storage time that is expressed as a Gaussian distribution with a prescribed maximum age of 3 years and a mean and standard deviation that can be specified. In contrast, the fracture-fed flow is instantaneously passed through the system (i.e. with a travel time of less than one month). The seepage and fracture-fed components are mixed before emerging at the drip. The drip is treated as being of an overflow type such that in a typical year the drip rate becomes very slow (matching our field observations detailed earlier), since the level in the feeding reservoir is insufficient to maintain the drip.

Input data for the hydrological model is derived from meteorological records and collections of rain waters for stable isotopes in Addis Ababa (latitude 9°N , longitude 38.73°E , altitude 2360 m). Although monthly isotopic data are available from 1961, the data collection is spasmodic until 1990 after which nearly continuous records have been kept. Figure 4a illustrates scatter plots of rainfall $\delta^{18}\text{O}$ composition versus rainfall amount. Significant relationships are found only with two months (April and June) when there is an inverse relationship (amount effect). Figure 4b shows that seasonal variations in $\delta^{18}\text{O}$ dominate over the amount effect, with lightest monthly mean isotopic composition in July and August. The model

is spun up from 1961 to 1989 using predictions from these relationships for April and June and the mean composition for each month otherwise. The amount of rainfall is adjusted from the Addis Ababa data by using a constant factor for each month (varying between 0.52 for August to 2.92 for November) as in Baker *et al.* (2007). In the period since 1990, the input isotopic values are adjusted to be those recorded in the month in question at Addis Ababa.

Model output demonstrates a reasonable agreement between modelled drip water $\delta^{18}\text{O}$ and actual modern stalagmite $\delta^{18}\text{O}$. Figure 5b presents the results of just one model run as an example. In the figure, the water isotope data are expressed with respect to VSMOW (mean -1.29‰); the calcite data have been expressed with respect to VPDB (mean -0.43‰) with an offset of -1.2‰ . At equilibrium at a temperature of 19°C , the calcite values would be expected to be 0.76‰ (Kim and O'Neil, 1997) or 1.15‰ (Friedman and O'Neil, 1977) lower than those of the co-existing water, whereas the best visual match, as in the figure corresponds to them being 1.2‰ higher. Hence it can be interpreted that the water must have evaporated by around $2\text{--}2.5\text{‰}$ between rainwater and stalagmite, possibly because of evaporation in the soil and near surface groundwater ($\sim 2\text{‰}$ enrichment with a 1 mm/day potential evaporation has been reported elsewhere, Hsieh *et al.*, 1998) or in the cave itself. The most important inference that can be made from the model is that there are significant deviations in the modelled drip water isotope composition, whereas rainfall amounts show much less interannual variation in this period, suggesting stalagmite $\delta^{18}\text{O}$ is likely to reflect

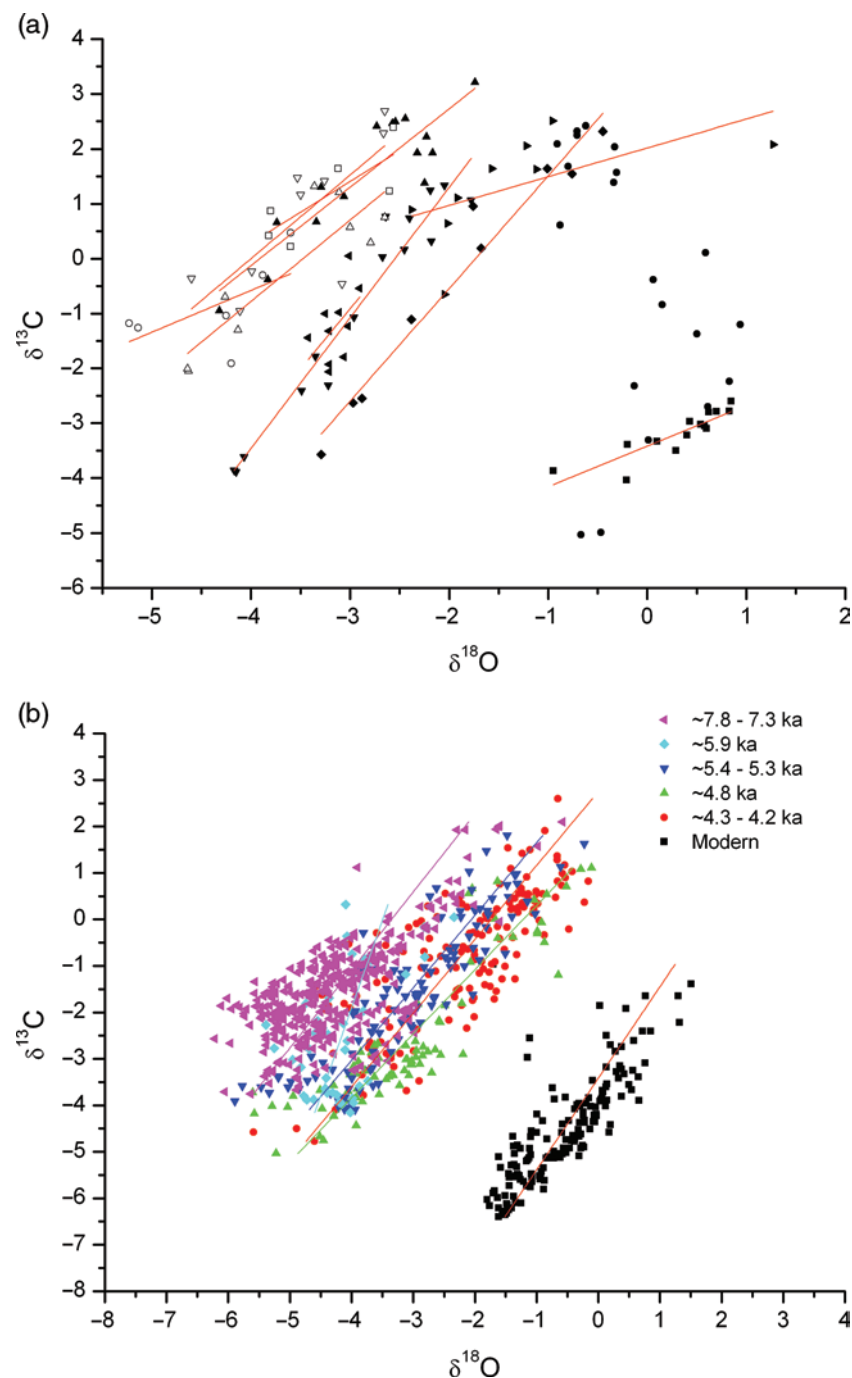


Figure 3. (a) $\delta^{13}\text{C}$ versus $\delta^{18}\text{O}$ along individual growth layers ('Hendy tests'). For location of Hendy tests see Figure 1. Ten out of eleven Hendy tests provide evidence of additional fractionation during drip water evolution down the stalagmite with typical gradients of $\delta^{13}\text{C}/\delta^{18}\text{O}$ of 0.5–2.4, indicative of kinetic fractionation similar to that under 'fast degassing' observed experimentally (1.4 ± 0.6) (Wiedner *et al.*, 2008). (b) $\delta^{13}\text{C}$ versus $\delta^{18}\text{O}$ for time series data presented in Figure 2 for each growth phase. Statistically significant correlations occur in all growth phases. The range of $\delta^{18}\text{O}$ within a growth phase is greater than that observed in an individual 'Hendy test'

differences in the relative amounts of rain that falls in the two rain seasons, rather than a simple total rainfall amount. For example, the model reproduces a broad maximum in isotope composition found in the speleothem between 1990 and 1997, followed by a sharp fall, and subsequent rise and fall. This fall in the late 1990s coincides with three years where the (isotopically heavy) spring rains failed and which lead to a widespread famine crisis in Ethiopia in 1997–1999. However, one must remember that the strong $\delta^{18}\text{O}$ – $\delta^{13}\text{C}$ covariation found in the speleothem data (Figure 3a) suggests that additional non-equilibrium fractionation is possible.

The model output was tuned to derive as close a range and timing as possible to the stalagmite sample. Model outputs are shown in Figure 5c, with the best fit to the range and timing in the stalagmite found by setting the lower threshold (infiltration to the seepage flow compartment of the aquifer) to between 40 and 60 mm per month, the upper threshold to ~ 170 mm per month, and the Gaussian parameters for residence time as 6 ± 6 months (as shown in Figure 5b). Periods with greatest differences between model and stalagmite occur around 1993 and 2002–2004; in both cases stalagmite $\delta^{18}\text{O}$ is $\sim 1\%$ lighter than that modelled but within the range of

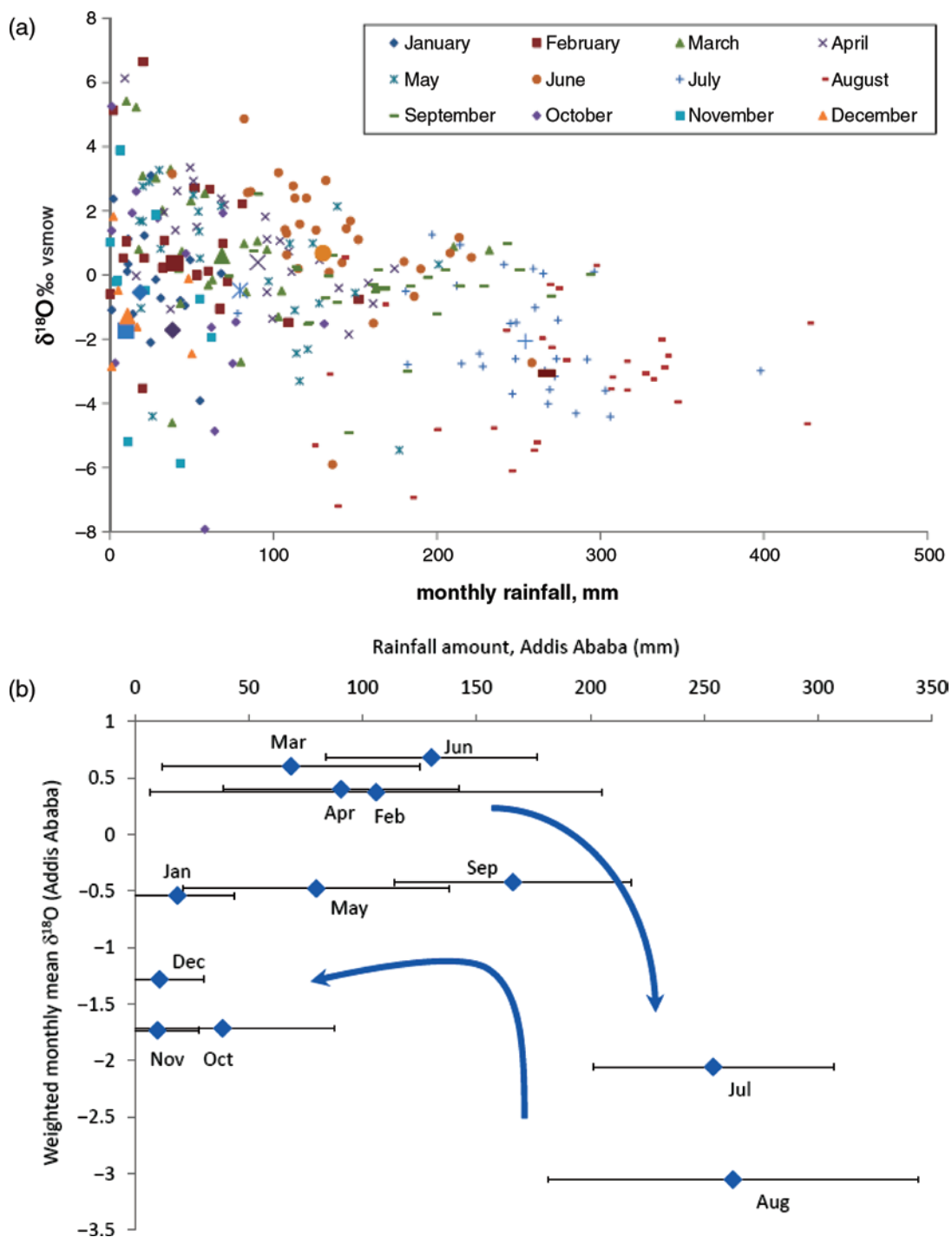


Figure 4. (a) All available monthly rainfall data at Addis Ababa since 1961 differentiated by month. Monthly means are shown as enlarged symbols. (b) Mean monthly rainfall amount versus weighted monthly mean $\delta^{18}O$. Arrows indicate the monthly evolution of rainfall isotopic composition over the summer rain period

variability of monthly mean rainfall. The cause of this disagreement is unknown, but in both 1993 and 2002 the $\delta^{18}O$ of summer precipitation at Addis Ababa was unusually heavy. The model therefore predicts heavier stalagmite $\delta^{18}O$ than observed: a simple explanation would be that isotopically lighter summer rainfall occurred at the study site compared to Addis Ababa in those years.

An overflow hydrological routing, combined with drip-rate being controlled by a limited storage reservoir, also explains the variable and non-linear growth rate time series. Stalagmite growth rate is controlled by the number of months of active drip water,

PCO_2 in incoming drip water versus cave atmosphere, and temperature (Dreybrodt, 1988). In our near cave-entrance site, and in a region of near constant surface temperature, primary controls will be drip water PCO_2 (which will be a function of both soil CO_2 and the degassing history of the drip-water, and will generate the low frequency variability in growth rate) and the volume of drip water supplied to the stalagmite in a year. The latter will be a function of rainfall amount and seasonality as well as antecedent stored water; the predominant control of water supply on growth rate generates the high frequency, non-linear, variability in growth rate.

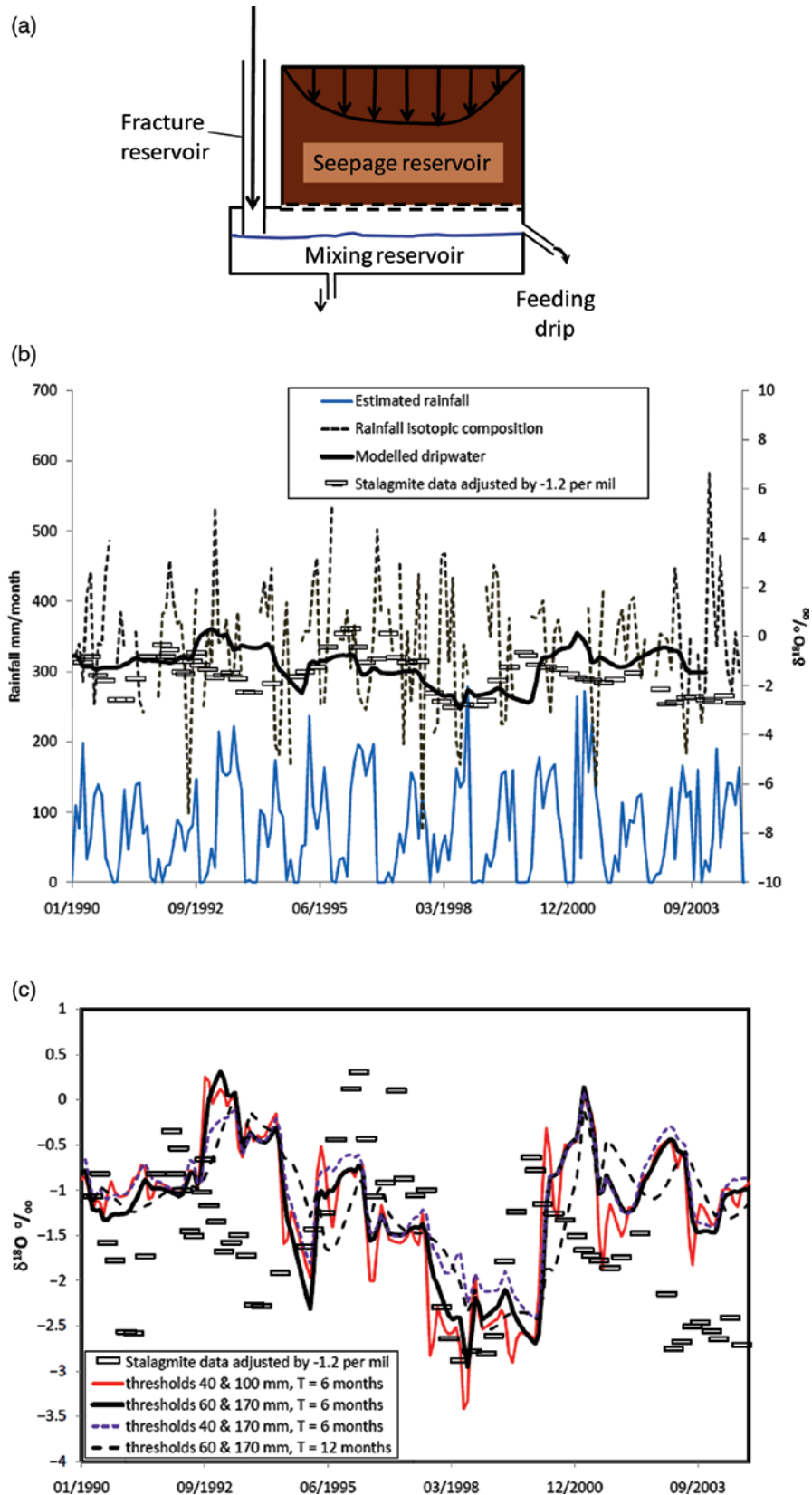


Figure 5. (a) Schematic of the hydrological model. Rainfall exceeding a lower monthly threshold recharges a seepage-flow reservoir within which there are varied flow velocities (arrows) and hence transit times. Where rainfall exceeds a higher threshold it is rapidly infiltrated through fractures and mixes with seepage water to supply the feeding drip at times of year where the total water supply is sufficient. (b) Model outputs and stalagmite isotopic composition compared with monthly rainfall isotopic compositions and amounts. The hydrological model output data for water stable isotopic composition are smoothed by a 2-month running mean (50% weighted from the current month t and 25% each from months $(t+1)$ and $(t-1)$), which approximates to the mean temporal smoothing of the speleothem data of 0.25 months. The decline in modelled $\delta^{18}\text{O}$ composition in the late 1990s can be seen to relate to the increased proportion of isotopically light rainfall. (c) Comparison of five different model outputs

Table 2. Spectral analysis

Bero-1	$\delta^{18}\text{O}$ periods (years)	Growth rate periods (years)
~7.8–7.3 ka	24–34 40–46	11–13 18–19 30–43
~5.4–5.3 ka	9 15–21	10–13 15–20
~4.3–4.2 ka	8 12–15	11–15 17–21
Ach-1		
~5.1–4.7 ka	18–21	18–21

Frequencies shown are those consistently significant at 95% confidence interval using rectangular, Welch I and Hanning windows, calculated using SPECTRUM (Schultz and Stattegger, 1997). Results are shown for both Bero-1 and previously published Ach-1 (Asrat *et al.*, 2007). The growth phases at ~4.8 and ~5.9 ka are of too short a duration (< 100 years) for spectral analysis.

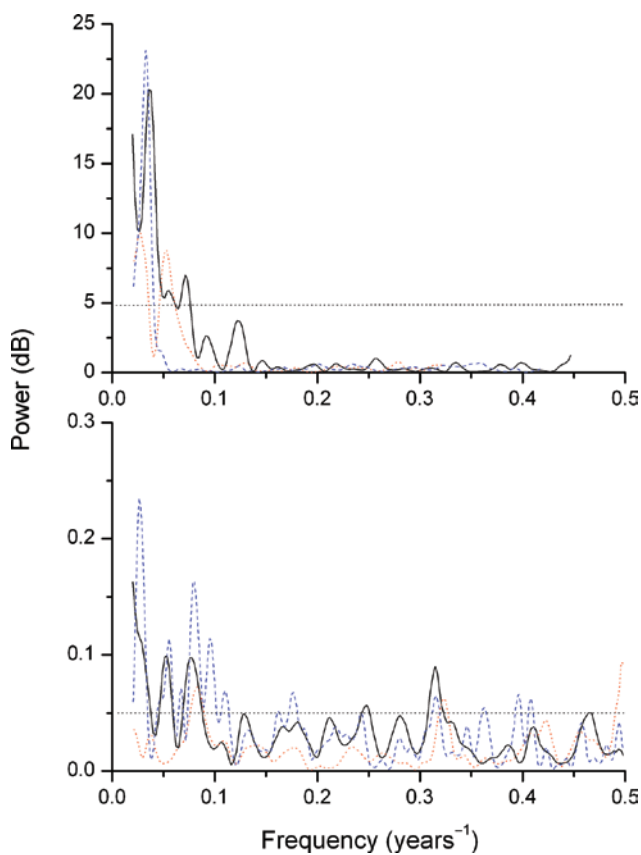


Figure 6. Example spectral analysis of $\delta^{18}\text{O}$ (top) and growth rate (bottom). In all cases a Hanning window was used. Solid line: ~4.3–4.2 ka growth. Dotted line: ~5.4–5.3 ka growth. Dashed line: ~7.8–7.3 ka growth. The strictest of the three 95% confidence levels is shown as a dotted line. Spectral peaks of frequency less than 0.02 (50 years) are not shown because of limited number of potential cycles represented

Conclusions

Both $\delta^{18}\text{O}$ and growth rate series exhibit persistent decadal-scale variability in both proxies throughout the Holocene. This is confirmed by statistically significant spectral periodicities of between 10 and 21 years (Table 2 and Figure 6). Additionally, isotopically lighter mean $\delta^{18}\text{O}$ is observed earlier in the Holocene, and likely reflects long-term orbital forcing, affecting the amount and/or isotopic signature of the summer rains (Olago *et al.*, 2007). The lower

$\delta^{18}\text{O}$ in the earlier Holocene, when rapid degassing is still possible (Figure 3a), suggests that changes in kinetic fractionation do not obscure the long-term source water $\delta^{18}\text{O}$ signal. Changes in the rate of degassing, if they did occur, might additionally contribute to our modelled $\delta^{18}\text{O}$ variability, accentuated in drier years with lower drip discharges and longer drip water evolution (Wiedner *et al.*, 2008).

Both $\delta^{18}\text{O}$ and growth rate proxies can therefore be interpreted in terms of rainfall amount; our forward model implies that negative isotopic shifts in $\delta^{18}\text{O}$ can be interpreted as either an intensification of summer rains or a failure of the spring rains. For the growth rate, the significant interannual variability can only be interpreted as years of extended drip water supply. Low-frequency variability in both $\delta^{18}\text{O}$ and growth rate is similar to that observed in limited instrumental series as well as our previously published mid-Holocene stalagmite record from the same region (Asrat *et al.*, 2007; see Table 1). This decadal-scale variability in both proxies indicates decadal variability in Ethiopian precipitation.

Decadal-scale variability in Ethiopian precipitation could be caused by one or several large-scale SST or atmospheric circulation anomalies. On decadal and multidecadal timescales, variability in cross-equatorial Atlantic SST gradients in the twentieth century (Chang *et al.*, 1997) has been suggested to contribute to long-term variability of rainfall in the Sahel and northeast South America (Folland *et al.*, 1986; Giannini *et al.*, 2003). The variable gradients may be attributable to an unstable thermodynamic ocean–atmosphere interaction between wind-induced heat fluxes and SST (Chang *et al.*, 1997). When the tropical North Atlantic is cool relative to the tropical South Atlantic, increased surface pressure gradient in the north forces the ITCZ to move south, resulting in dry conditions in North Africa and wetter conditions in northeast South America (Chang *et al.*, 2008; Lu and Dong, 2008). Links between Ethiopian rainfall and SSTs or atmospheric circulation might also be associated with changes in the position of the ITCZ or variations in the Indian Ocean Dipole (Vuille *et al.*, 2005), but this has not yet been investigated. However, it seems to be at least a potential explanation for the decadal variability recorded in our proxy data throughout the Holocene. Decadal to multidecadal stable isotopic variability in four Holocene coral skeletons from the Dominican Republic (Greer and Swart, 2006) provides further evidence that the fluctuation of the ITCZ associated with decadal Atlantic SST variability might play an important role across the Atlantic basin (Lu and Dong, 2008). Finally, subtle changes in spectral frequency are observed in the earliest growth phases of our stalagmite, at a time when solar insolation was higher, which might imply subtle changes in ocean–atmospheric circulation at that time.

Acknowledgements

We thank Natural Environment Research Council, The Leverhulme Trust and START/PACOM for funding, and Phil Hopley for his review comments. Paul Hands performed stalagmite sectioning and thin sectioning and Peter Wynn prepared samples for ^{14}C analysis. Hilary Sloane undertook the stable isotope measurements.

References

- Asrat A, Baker A, Umer M, Leng MJ, van Calsteren P and Smith CL (2007) A high-resolution multi-proxy stalagmite record from Mechara, southeastern Ethiopia: Paleohydrological implications for speleothem paleoclimate reconstruction. *Journal of Quaternary Science* 22: 53–63.

- Asrat A, Baker A, Leng MJ, Gunn J and Umer M (2008) Environmental monitoring in the Mechara caves, southeastern Ethiopia: Implications for speleothem palaeoclimate studies. *International Journal of Speleology* 37: 207–220.
- Baker A, Bradley C (2010) Modern stalagmite $\delta^{18}\text{O}$: Instrumental calibration and forward modelling. *Global and Planetary Change* 71: 201–206
- Baker A, Asrat A and Mohammed M (2005) Expedition report to the Mechara caves, southeastern Ethiopia. *Speleology* 5: 8–20.
- Baker A, Asrat A, Fairchild IJ, Leng MJ, Wynn PM, Bryant C *et al.* (2007) Analysis of the climate signal contained within $\delta^{18}\text{O}$ and growth rate parameters in two Ethiopian stalagmites. *Geochimica et Cosmochimica Acta* 71: 2975–2988.
- Block P, Rajagopalan B (2007) Interannual variability and ensemble forecast of Upper Blue Nile Basin Kiremt season precipitation. *Journal of Hydrometeorology* 8: 327–343.
- Camberlin P, Philippon N (2002) The East African March–May rainy season, its teleconnections and predictability over the 1968–1997 period. *Journal of Climate* 15: 1002–1019.
- Chang P, Ji L and Li H (1997) A decadal climate variation in the tropical Atlantic Ocean from thermodynamic air–sea interactions. *Nature* 385: 516–518.
- Chang P, Zhang R, Hazeleger W, Wen C, Wan X, Ji L *et al.* (2008) Oceanic link between abrupt changes in the North Atlantic Ocean and the African monsoon. *Nature Geoscience* 1: 444–448.
- Chou C, Tu J-Y and Tan P-H (2007) Asymmetry of tropical precipitation change under global warming. *Geophysical Research Letters* 34: L17708.
- Conway D, Mould C and Bewket W (2004) A century of climate observations at Addis Ababa, Ethiopia. *International Journal of Climatology* 24: 77–91.
- Diro GT, Black E and Grimes DIF (2008) Seasonal forecasting of Ethiopian spring rains. *Meteorological Applications* 15: 73–83.
- Dreybrodt W (1988) *Processes in Karst Systems*. Berlin: Springer-Verlag, 288 pp.
- Edwards RL, Chen JH and Wasserburg GJ (1987) ^{238}U – ^{234}U – ^{232}Th – ^{230}Th systematics and the precise measurement of time over the last 500 000 years. *Earth and Planetary Science Letters* 81: 175–192.
- Fairchild IJ, Tuckwell GW, Baker A and Tooth AF (2006) Modelling of dripwater hydrology and hydrogeochemistry in a weakly karstified aquifer (Bath, UK): Implications for climate change studies. *Journal of Hydrology* 321: 213–231.
- Folland CK, Palmer TN and Parker DE (1986) Sahel rainfall and worldwide sea temperatures. *Nature* 320: 602–607.
- Friedman I, O’Neil JR (1977) *Compilation of Stable Isotope Fractionation Factors of Geochemical Interest*. US Geological Survey Professional paper 440-KK, 49 pp.
- Genty D, Baker A, Massault M, Proctor C, Gilmour M, Pons E *et al.* (2001) Stalagmite dead carbon proportion variation: Paleodissolution process and soil organic matter dynamics recorder – implications for ^{13}C variations in stalagmites. *Geochimica et Cosmochimica Acta* 65: 3443–3457.
- Giannini A, Saravanan R and Chang P (2003) Oceanic forcing of Sahel rainfall on interannual to interdecadal time scales. *Science* 302: 1027–1030.
- Glantz MH (1996) *Currents of Change: El Niño’s Impact on Climate and Society*. Cambridge: Cambridge University Press.
- Greer L, Swart PK (2006) Decadal cyclicity of regional mid-Holocene precipitation: Evidence from Dominican coral proxies. *Paleoceanography* 21, PA2020.
- Gunn J, Baker A and Asrat A (2009) Caves of Mechara: The Millennium Expedition to Ethiopia. *National Speleological Society News* June: 4–7.
- Hsieh JCC, Chadwick OA, Kelly EF and Savin SM (1998) Oxygen isotopic composition of soil water: Quantifying evaporation and transpiration. *Geoderma* 82: 269–293.
- Kim ST, O’Neil JR (1997) Equilibrium and non-equilibrium oxygen isotope effects in synthetic carbonates. *Geochimica et Cosmochimica Acta* 61: 3461–3475.
- Korecha D, Barnston AG (2007) Predictability of June to September rainfall in Ethiopia. *Monthly Weather Review* 135: 628–650.
- Lu R-Y, Dong B-W (2008) Response of the Asian summer monsoon to a weakening of Atlantic thermohaline circulation. *Advances in Atmospheric Science* 25: 723–736.
- Nicholson SE (2000) The nature of rainfall variability over Africa on time scales of decades to millennia. *Global Planetary Change* 26: 137–158.
- Olago DO, Umer M, Ringrose S, Huntsman-Mapila P, Sow EH and Damnati B (2007) Palaeoclimate in Africa: An overview since the Last Glacial Maximum. In: Otter L, Olago DO and Niang I (eds) *Global Change Processes and Impacts in Africa: A Synthesis*. Washington: START 346.
- Rowell DP, Ininda JM and Ward MN (1994) The impact of global sea surface temperature patterns on seasonal rainfall in East Africa. In: *Proceedings, International Conference on Monsoon Variability and Prediction, Trieste, Italy*. World Climate Research Programme, Series Report 84. WMO, 6660672.
- Schultz M, Statterger K (1997) Spectrum: Spectral analysis of unevenly spaced paleoclimate time series. *Computers and Geosciences* 23: 929–945.
- Slota PJ, Jull AJT, Linick TW and Toolin LJ (1987) Preparation of small samples for ^{14}C accelerator targets by catalytic reduction of CO. *Radiocarbon* 29: 303–306.
- Smart PL, Friedrich H (1987) Water movement and storage in the unsaturated zone of a maturely karstified aquifer, Mendip Hills, England. *Proceedings of the Conference: Environmental Problems in Karst Terrains and their Solution, Bowling Green, Kentucky*. National Water Well Association, USA, 57–87.
- Tan M, Baker A, Genty D, Smith C, Esper J and Cai B-G (2006) Applications of stalagmite laminae to paleoclimate reconstructions: Comparison with dendrochronology/ climatology. *Quaternary Science Reviews* 25: 2103–2117.
- Vuille M, Werner M, Bradley RS, Chan RY and Keimeg F (2005) Stable isotopes in East African precipitation record Indian Ocean zonal mode. *Geophysical Research Letters* 32: L21705.
- Wiedner E, Scholtz D, Mangini A, Polag D, Mühlinghaus C and Segl M (2008) Investigation of the stable isotope fractionation in speleothems with laboratory experiments. *Quaternary International* 187: 15–24.